Applied Energy 339 (2023) 120984

Contents lists available at ScienceDirect

Applied Energy

journal homepage: www.elsevier.com/locate/apenergy

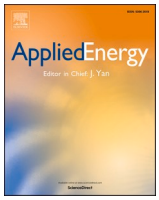

Multi-layer energy management of smart integrated-energy microgrid systems considering generation and demand-side flexibility

Hamid Karimi , Shahram Jadid *

Department of Electrical Engineering, Center of Excellence for Power System Automation and Operation, Iran University of Science and Technology, Iran

HIGHLIGHTS

- Proposing a multi-layer framework for operation scheduling of SIEMS.
- Considering the electrical and thermal generation flexibility in the second stage.
- Three new indexes are introduced to evaluate the flexibility of the system.
- Hybrid min–max and max–min approach is developed to provide demand-side flexibility.
- The water storage system are integrated into the system.

ARTICLE INFO

Keywords:
Smart integrated energy microgrid system
System flexibility
Renewable energy resources
Energy storage system
Peak load reduction

ABSTRACT

This paper proposes a stochastic framework for the operation scheduling of integrated renewable-based energy microgrid systems. The proposed model presents comprehensive scheduling that simultaneously considers total generation costs, generation flexibility, and demand-side flexibility. This operation management approach is modeled as the tri-layer framework. At the first layer, the microgrid system attempts to minimize daily operation costs considering the probabilistic behavior of renewable generation, signal prices, and loads. The desalination unit and water tank storage have been incorporated into the proposed structure to supply potable water for the system. The second layer reschedules the obtained management of the first layer to increase the thermal flexibility and electrical flexibility of local generation resources. To this end, the integrated energy system tries to maximize the spinning reserve of the local energy resources in the second layer. The last layer is responsible to increase demand-side flexibility. In this layer, a hybrid max–min and min–max approach is developed to uniform the load profile by demand-side management programs. The proposed framework is applied to the general structure of energy systems and the day-ahead results demonstrate that the electrical generating flexibility index and thermal generating flexibility index are improved by 22.98% and 34.64% in the proposed model.

1. Introduction

The environmental pollution of fossil fuels and the increasing acceleration of the depletion of fossil-based fuels are two main challenge for humanity [1,2]. The significant contribution of fuel-based power plants is the major cause for the environmental challenges [3]. Global warming and climate change are the most important threats to fossil fuel combustion. [4,5]. In December 2015, all parties pledged to strengthen and increase their efforts to decrease the carbon capture through the Paris Agreement [6]. Integration of renewable energy resources (RES) is one of the main solutions to achieve the goals of the Paris Agreement [7].

With the high penetration of RES, the future energy system requires an extremely strong interaction between different energy sectors such as electricity, heating, and cooling [8,9]. The integrated energy systems (IES) can cope fluctuation of RES in an efficient way to provide the decarbonization opportunity for smart energy systems [10]. Smart integrated energy microgrid systems (SIEMS) connect the energy-consuming sectors to the upstream network. This integration enhances the efficiency, flexibility, and resilience of the system [11].

Various research works studied the operation scheduling of smart integrated energy microgrid systems. Authors in [12] developed multi-objective decision-making that applied the epsilon constraint method to minimize the total operating costs and freshwater extraction from underground resources simultaneously. A multi-time scale framework

* Corresponding author.
E-mail addresses: H_karimi@elec.iust.ac.ir (H. Karimi), Jadid@iust.ac.ir (S. Jadid).

https://doi.org/10.1016/j.apenergy.2023.120984
Received 20 December 2022; Received in revised form 3 March 2023; Accepted 13 March 2023
Available online 23 March 2023

Nomenclature

Abbreviations

AC	absorption chiller
ADFPPI	average demand-side flexibility during peak period index
AEGFI	average electrical generation flexibility index
ATGFI	average thermal generation flexibility index
CHP	combined heat and power
DR	demand response
EC	electric chiller
EESS	electrical energy storage system
ESS	energy storage system
EGF	electrical generation flexibility
ISC	ice storage conditioner
IES	integrated energy system
MILP	mixed-integer linear problem
PDF	probability distribution function
RES	renewable energy resources
SIEMS	smart integrated energy microgrid system
TGF	thermal generation flexibility

Indexes

c	ISC index
e	index of electrical ESS/DR
h	index of thermal ESS/DR
i	index of electrical/thermal/cooling devices
t	index of times
v	index of PEV
s	index of scenarios

Parameters

A^{pv}	photovoltaic panels area
$A^{s,w}$	cross-section of water storage
B^{pv}	number of photovoltaic panels
COP^{ac}	constants performance for AC
COP^{ec}	constants performance of EC
COP^{isc}	constants performance ISC
$CR_{dr}^{e,up}$	upward cost of DR for electrical load
$CR_{dr}^{e,down}$	downward cost of DR for electrical load
$CR_{dr}^{h,up}$	upward cost of DR for thermal load
$CR_{dr}^{h,down}$	downward cost of DR for thermal load
$E_{\min}^{i}$	lower bound of electrical energy in ESS i
$E_{\max}^{i}$	upper bound of heat energy in ESS i
g^{w}	earth gravity
$G_{\max}^{chp}$	upper bound of input gas to CHP
$G_{\max}^{boiler}$	upper bound of input gas to boiler
$H_{\max}^{boiler}$	maximum output heat of boiler
$H_{\max}^{ac}$	maximum input heat of absorption chiller
$I_{t,s}^{pv}$	solar emission at time t
LHV	low calorific value of natural gas
$L_{\max}^{grid}$	maximum imported power
L_{t}^{i}	load profile
L_{t}^{wl}	water consumption
$L_{\max}^{s,w}$	Upper bound of water in storage tank
$LL^{w,w}$	water reservoir level
$LL^{g,w}$	place height for water tank
$MRL^{i,up}$	maximum shifted-up for DR
$MRL^{i,down}$	maximum shifted-down for DR
$N^{pv,mpt}$	maximum power temperature coefficient of PV
$P_{\max}^{i,ch}$	charging power upper-bound
$P_{\max}^{i,disch}$	discharging power upper-bound
$P_{\max}^{h}$	maximum power transmission limit of heat pipe
P_{wt}^{r}	rated power of wind turbine
$P_{\max}^{ec}$	upper bound of input power to EC
$P_{\max}^{pev,ch}$	charging power upper-bound of PEV
$P_{\max}^{pev,disch}$	discharging power upper-bound of PEV
$P^{pev,tr}$	power consumption of PEV during travel
$Q_{\max}^{d,w}$	capacity of desalination
$Q_{\max}^{w,ch}$	maximum charging measure of water storage
$Q_{\max}^{w,disch}$	maximum discharging measure of water storage
$T^{pv,c}$	standard temperature
$SOC_{\min}^{pev}$	minimum SOC for PEV
$SOC_{\max}^{pev}$	maximum SOC for PEV
U_{em}^{g}	CO_2 emission coefficient for main grid
U_{em}^{boiler}	CO_2 emission coefficient for boiler unit
U_{em}^{chp}	CO2 emission coefficient for CHP unit
$V_{t,s}^{ac,wt}$	wind speed at time t
$V^{ci,wt}$	cut-in speed of wind turbine
$V^{co,wt}$	cut-out speed of wind turbine
$V^{rr,wt}$	rated speed of wind turbine
$p_{\max}^{gas}$	maximum imported gas
ρ^{w}	water density
λ_{t}^{g}	natural gas prices
π_{t}^{e}	electricity price
$\Delta D_{t,v}^{pev}$	traveling distance
$\eta^{p,w}$	water pump efficiency
η_{v}^{pev}	PEV efficiency
$\eta_{v}^{pev,ch}$	charging efficiency of PEV
$\eta_{v}^{pev,disch}$	discharging efficiency of PEV
$\eta^{i,disch}$	discharging efficiency of ESS i
$\eta^{i,ch}$	charging efficiency of ESS i
η^{boiler}	boiler efficiency
$\eta^{e,chp}$	gas to electricity efficiency of CHP
$\eta^{h,chp}$	gas to heat efficiency of CHP
$\eta^{d,w}$	efficiency of desalination

Variables

$Cost^{grid}$	cost of purchasing power from the upstream network
$Cost^{CHP}$	cost of CHP unit
$Cost^{boiler}$	cost of boiler
$Cost^{EDR}$	electrical DR cost
$Cost^{HDR}$	thermal DR cost
C_{t}^{ec}	output cooling of EC
C_{t}^{ac}	output cooling of AC
ES_{t}^{i}	stored energy in ESS i
$EE_{t}^{i,ch}$	binary variable for ESS i
$EE_{t}^{i,disch}$	binary variable for ESS i
G_{t}^{chp}	consumed natural gas by CHP
G_{t}^{boiler}	consumed natural gas by boiler
H_{t}^{boiler}	output heat power of boiler
H_{t}^{ac}	input heat to absorption chiller
$II_{t}^{i,down}$	binary variable for shift down for DR programs
$II_{t}^{i,up}$	binary variable for shift up for DR programs
$L_{t}^{s,w}$	water level of the storage
P_{t}^{g}	purchasing power from the main grid
$P_{t}^{e,chp}$	output electrical power of CHP
$P_{t}^{h,chp}$	output heat power of CHP
$P_{t,s}^{wt}$	output power of wind turbine
$P_{t,s}^{pv}$	output power of photovoltaic cells
P_{t}^{ec}	input power to electrical chiller
$PD_{t}^{i,down}$	shifted down power of DR programs

$PD_t^{i,up}$	shifted up power of DR programs
$P_t^{i,ch}$	charging power of ESS i
$P_t^{i,disch}$	discharging power of ESS i
$P_t^{pev,ch}$	charging power of PEV
$P_t^{pev,disch}$	discharging power of PEV
$PP_{t,v}^{pev,ch}$	binary variable for PEV charging
$PP_{t,v}^{pev,disch}$	binary variable for PEV discharging
$P_t^{pw,w}$	power consumption of water well pump
$P_t^{ps,w}$	power consumption of water storage pump
$P_t^{d,w}$	power consumption of water desalination unit
$P_t^{water,w}$	consumed electricity by the water network
P_t^{isc}	input power to ISC
P_t^{gas}	input gas from gas network
$Q_t^{w,w}$	ground water extraction
$Q_t^{d,w}$	water product of desalination unit
$Q_t^{w,ch}$	charging variable of water tank
$Q_t^{w,disch}$	discharging variable of water tank
SOC_t^{pev}	stored energy in PEV
$WW_t^{w,ch}$	binary variable of water storage charging
$WW_t^{w,disch}$	binary variable of water storage discharging

was presented in [13] to decrease the day-ahead operation cost of the energy system. The proposed structure integrated the electrical, heating, and cooling sectors, while water management was not developed in the proposed model. Wang et al. in [14] suggested a two-stage stochastic approach to handle the uncertain behavior of parameters in the operation scheduling of IES. Ref. [15] proposed a genetic algorithm for the operation scheduling of IES to study the hybrid energy storage systems impacts. A multi-stage stochastic energy scheduling was developed in [16] that optimized the operation cost, reliability problems, and flexibility indexes simultaneously. Although the uncertainty of demands, RES, and signal prices had been considered, the water system was not developed.

New challenges had created in the operation scheduling of SIEMS because of the high penetration of RES and their probabilistic behaviors [17]. The flexibility concept discusses the ability of SIEMS to manage short-term and long-term changes [18]. The greater flexibility provides more ability for SIEMS for reliable and cost-effective management. The energy storage systems (ESS) and combined heat and power (CHP) can create production flexibility for SIEMS. Honarmand et al. [19] integrated the ESS into the SIEMS to present long-term planning where the ESS provides the required generation flexibility. Tiwari et al. [20] proposed cooperative energy management for the operating management of neighbor SIEMS to create more flexibility. However, the thermal and electrical generation flexibilities were not considered as the objective function. Besides, the water sector was ignored. Ref. [21] developed mixed-integer linear programming (MILP) considering the uncertainty of SIEMS to present a comprehensive model for the system design. However, the thermal and electrical generation flexibilities were not considered.

The energy storage systems can significantly increase the generation flexibility of SIEMS by charging and discharging cycles. They can store energy when the SIEMS has surplus power by charging mode. The stored energy can be used during peak periods or when the renewable generation decreased from the forecasted values. Rezaei et al. [22] investigated the impact of energy storage systems on the peer-to-peer energy trading of SIMES. Ref. [23] studied the efficiency of heat storage on the operation performance of residential energy systems in different seasons. However, the water management system was not considered. A four-objective optimization framework has been suggested in [24] to evaluate the impacts of ESS and the number of electric vehicles on the emission reduction and dependency index of SIEMS. However, the generation flexibility and the flexibility of end-users had not directly studied. Wen et al. [25] applied the grasshopper optimization algorithm to study the performance of cooling storage systems and compressed-air energy storage systems in the management of SIMES. The suggested approach considered the probabilistic behavior of wind energy and photovoltaic energy to meet the required loads. However, demand-side flexibilities were ignored by this study. A probabilistic approach had been suggested in [26] that modeled the participation of SIEMS in electricity, heat, and natural gas markets. The SIEMS utilized different converters and energy storage systems to present flexible and reliable scheduling. However, the role of the water tank storage system, electrical and thermal demand-side flexibilities were not studied.

Electrical and thermal demand response programs (DR) have been known as one of the solutions to provide demand-side flexibility for SIES. Through DR programs, the customers can shift their loads when the generation of RES changes from the forecasted values. Thang et al. [27] integrated demand-side management to enhance the demand-side flexibility of SIES. The authors utilized the probabilistic method to model the uncertainty of RES, load demands, and signal prices. However, water management was not studied. Ref. [28] presented a multi-stage stochastic model to study the impact of demand-side programs in the scheduling planning of SIEMS by binary genetic algorithm. However, the thermal and electrical generation flexibilities were not deployed. Ref. [29] studied the long-term effect of energy storage systems and DR programs on the operation scheduling of SIES. The proposed model is modeled as multi-objective framework that minimized the operating costs and environmental problems simultaneously. However, the generation flexibility for electrical and thermal sections were not investigated. A day-ahead energy management framework has been developed in [30] to evaluate the role of demand-side management in economic scheduling. Although the uncertain behavior of RES and load demand had been managed by the ESS and demand-side management, the thermal and electrical generation flexibilities were not considered.

According to the literature, the DR programs make available the opportunity for cost-reduction by the load shifting from peak hours to off-peak hours. Given that the market prices during off-peak hours are low, the uncoordinated demand-side management may increase the peak load during off-peak hours. In this case, the SIEMS should increase the local generation to supply the required demands. So, it decreases the spinning reserve that significantly effected on the generation flexibility. Therefore, this paper suggests a stochastic tri-layer optimization that optimizes the generation and demand-side flexibility. The proposed model uniforms the load profile by the coordinated DR programs and prevents new peak load. Therefore, it increases the flexibility of SIEMS and facilitates the integration of RES in the distribution systems. According to the literature, the major contributions of the paper are listed as:

1. Presenting a multi-layer approach that optimizes the system flexibility and operation costs simultaneously. In the proposed model, each layer emphasizes different characteristics of SIEMS.
2. The thermal and electrical generation flexibilities of the system are optimized at the second stage to facilitate renewable generation integration in the distribution systems. However, this layer provides more flexibility that enhances the ability of SIEMS to manage unanticipated changes.
3. A hybrid min–max and max–min approach is developed to provide demand-side flexibility in the last layer. Also, this layer improves the system efficiency by peak load reduction and load factor improvement.

4. Three new indexes are introduced to evaluate the electrical generation flexibility, thermal-generation flexibility, and demand-side flexibility of the SIEMS.

2. Smart integrated energy system structure

The proposed structure of the smart integrated energy system is shown in Fig. 1. The proposed framework integrates the water, cooling, heating, and electrical sections to enhance the system's efficiency. In the proposed structure, the ESS, electric vehicles, and electrical demand-side management provide the required flexibility in the electrical section. In the heating section, the thermal energy storage systems and thermal DR program are the solutions to create thermal flexibility for the heating sector. Also, the ice storage conditioner (ISC) and water storage provide the required flexibility for cooling and water sections, respectively. The CHP unit links the electrical and heating sections together. The electric chiller (EC) and absorption chiller (AC) connected the cooling sector to the electrical and heating sectors, respectively. Also, desalination links the electrical and water sections together. According to Fig. 1, the SIEMS can supply the required freshwater from the underground resources or desalination unit.

2.1. Electrical and thermal DR programs

The electrical and thermal DR programs are modeled according to (1)–(4) [31,32]:

$$\sum_t PD_t^{i,up} = \sum_t PD_t^{i,down} \tag{1}$$

$$0 \leqslant PD_t^{i,down} \leqslant MRL^{i,down} L_t^i II_t^{i,down} \tag{2}$$

$$0 \leqslant PD_t^{i,up} \leqslant MRL^{i,up} L_t^i II_t^{i,up} \tag{3}$$

$$0 \leqslant II_t^{i,up} + II_t^{i,down} \leqslant 1 \tag{4}$$

Equation (1) shows that the SIEMS participates in the shiftable DR programs, where the shifted-up and shifted-down powers should be the same. The bounds of hourly load shifting are limited by (2) and (3). Finally, Eq. (4) determines the shifted-up or shifted-down modes. The index $i \in e, h$ refers to the DR program types, where h, and e show the thermal and electrical DR programs, respectively.

2.2. Electrical, heat, and cooling energy storage systems

The formulations of energy storage system are demonstrated in (5)–(10) [33,34].

$$0 \leqslant P_t^{i,ch} \leqslant P_{\max}^{i,ch} EE_t^{i,ch} \tag{5}$$

$$0 \leqslant P_t^{i,disch} \leqslant P_{\max}^{i,disch} EE_t^{i,disch} \tag{6}$$

$$ES_t^i = ES_{t-1}^i + (P_t^{i,ch} \eta^{i,ch}) - \left(\frac{P_t^{i,disch}}{\eta^{i,disch}}\right) \tag{7}$$

$$E_{\min}^i \leqslant ES_t^i \leqslant E_{\max}^i \tag{8}$$

$$0 \leqslant EE_t^{i,ch} + EE_t^{i,disch} \leqslant 1 \tag{9}$$

$$ES_1^i = ES_{24}^i \tag{10}$$

Equations (5) and (6) show the bounds of charging and discharging powers. The SoC of storage systems is shown in Eq. (7). The minimum and the maximum stored energy is developed by (8). Equation (9) determines the charging or discharging modes at time t. Finally, Eq. (10) shows that the final stored energy in storage systems should be the equal to the initial energy. In the above formulation, the index $i \in e, h, c$ refers to the storage system types, where e, h, and c show the electrical, thermal, and cooling storage systems, respectively.

2.3. Renewable energy resources

The generating power of photovoltaic panels is calculated by (11). A stochastic approach is used to handle the solar radiation scenarios. Beta probability distribution function (PDF) is developed for scenario generation of solar radiations. The Beta PDF is modeled by (12) to (14) [35].

$$P_{t,s}^{pv} = B^{pv} A^{pv} I_{t,s}^{pv} (1 + N^{pv,mpt} (T^{pv,c} - T_t^{pv,out})) \tag{11}$$

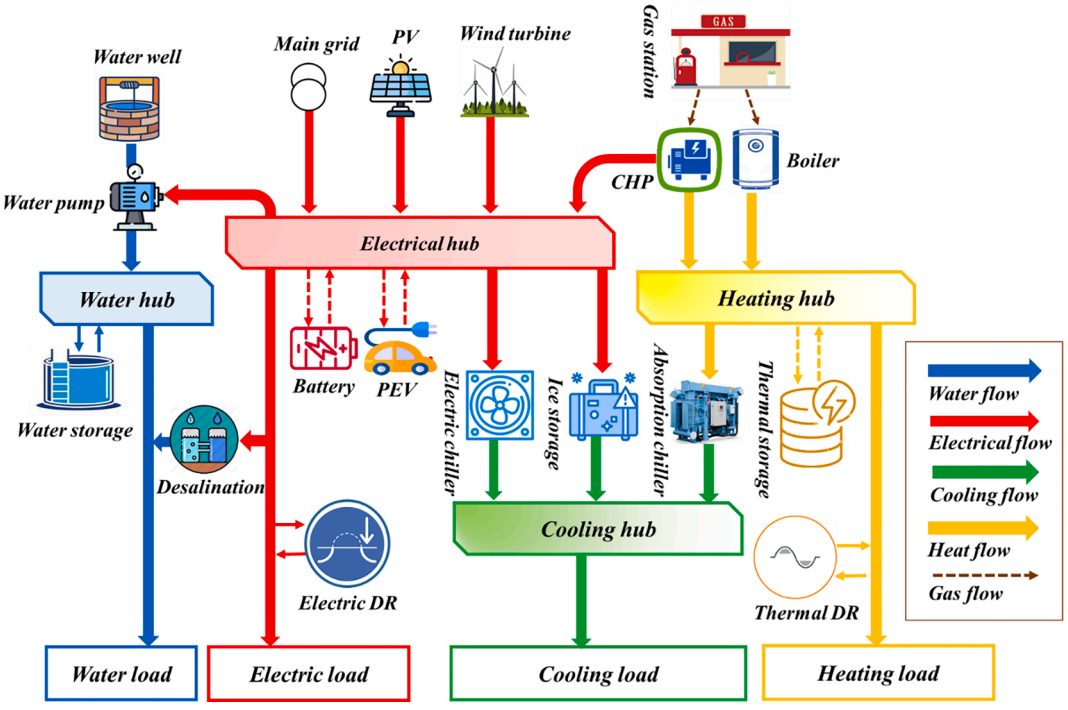

Fig. 1. Structure of smart integrated system.

$$PDF(x) = \frac{\Gamma(\alpha+\beta)}{\Gamma(\alpha)\Gamma(\beta)} x^{\alpha-1}(1-x)^{\beta-1} \tag{12}$$

$$\beta = (1-\mu)\left(\frac{\mu(1-\mu)}{\delta^2} - 1\right) \tag{13}$$

$$\alpha = \frac{\mu\beta}{1-\mu} \tag{14}$$

where α and β refer to the shape parameters of the gamma function Γ (α, $\beta \geq 0$). Equations (13) and (14) show that shape parameters are calculated by standard deviation δ and mean value μ.

However, the generating power of wind turbines is deliberated by (15). The Weibull PDF is considered to generate the related wind speed scenarios according to (16)–(18).

$$P_{t,s}^{wt} = \begin{cases} 0, & V_{t,s}^{ac,wt} \leqslant V^{ci,wt} \text{ or } V^{co,wt} \leqslant V_{t,s}^{ac,wt} \\ P^{r,wt}\dfrac{V_{t,s}^{ac,wt} - V^{ci,wt}}{V^{rr,wt} - V^{ci,wt}}, & V^{ci,wt} \leqslant V_{t,s}^{ac,wt} \leqslant V^{rr,wt} \\ P^{r,wt}, & V^{rr,wt} \leqslant V_{t,s}^{ac,wt} \leqslant V^{co,wt} \end{cases} \tag{15}$$

$$PDF(f) = \frac{k}{c}\left(\frac{f}{c}\right)^{k-1} \exp\left(-\left(\frac{f}{c}\right)\right) \tag{16}$$

$$k = \left(\frac{\delta}{\mu}\right)^{-1.086} \tag{17}$$

$$c = \frac{\mu}{\Gamma\left(1+\frac{1}{k}\right)} \tag{18}$$

where k and c refer to the shape parameters of Weibull PDF. Equations (13) and (14) show that the shape parameters of Weibull PDF that calculated by standard deviation δ and mean value μ

2.4. Plug-in electric vehicle

Charging power and discharging power constraints of electric vehicles have been demonstrated in (19) and (20). The state of charge of electric vehicles at time t is calculated by (21). Equation (22) determines the acceptable ranges of state of charge. The consumed energy in traveling mode is calculated by (23). Finally, Eq. (24) determines the charging or discharging modes [36].

$$0 \leqslant P_{t,v}^{pev,ch} \leqslant P_{\max}^{pev,ch} PP_{t,v}^{pev,ch} \tag{19}$$

$$0 \leqslant P_{t}^{pev,disch} \leqslant P_{\max}^{pev,disch} PP_{t,v}^{pev,disch} \tag{20}$$

$$SOC_{t,v}^{pev} = SOC_{t-1,v}^{pev} + (P_{t,v}^{pev,ch}\eta_{v}^{pev,ch}) - \left(\frac{P_{t,v}^{pev,disch}}{\eta_{v}^{pev,disch}}\right) - P_{t,v}^{pev,tr} \tag{21}$$

$$SOC_{\min}^{pev} \leqslant SOC_{t,v}^{pev} \leqslant SOC_{\max}^{pev} \tag{22}$$

$$P_{t,v}^{pev,tr} = \Delta D_{t,v}^{pev} \times \eta_{v}^{pev} \tag{23}$$

$$0 \leqslant PP_{t,v}^{pev,ch} + PP_{t,v}^{pev,disvh} \leqslant 1 \tag{24}$$

2.5. Electrical power balances and other related constraints

The electrical power balance shows that the electrical generation and load of SIEMS must be the same at each time slot. Equation (25) shows the electrical power balance in the SIES.

$$P_t^g + \sum_s \rho_s (P_{t,s}^{pv} + P_{t,s}^{wt}) + P_t^{e,chp} + PD_t^{e,down} + P_t^{e,disch} + \sum_v P_{t,v}^{pev,disch} = \sum_s \rho_s L_{t,s}^{e} + PD_t^{e,up} + P_t^{e,ch} + \sum_v P_{t,v}^{pev,ch} + P_t^{isc} + P_t^{ec} + P_t^{water,w} \tag{25}$$

Also, the generated electricity of the CHP unit is determined by (26). The input power to ISC is limited by (27). Equation (28) presents the electrical consumption bounds of electric chiller. Finally, the minimum and maximum purchasing/selling power from/to the main grid are presented in (29).

$$P_t^{e,chp} = G_t^{chp} LHV \eta^{e,chp} \tag{26}$$

$$0 \leqslant P_t^{isc} \leqslant P_{\max}^{isc} \tag{27}$$

$$0 \leqslant P_t^{ec} \leqslant P_{\max}^{ec} \tag{28}$$

$$-L_{\max}^{grid} \leqslant P_t^{g} \leqslant L_{\max}^{grid} \tag{29}$$

2.6. Heating balances and other related constraints

Equation (30) shows that the heat generation and thermal loads of SIEMS should be equal at each time slot [35].

$$P_t^{h,chp} + H_t^{boiler} + PD_t^{h,down} + P_t^{h,disch} = L_t^{h} + PD_t^{h,up} + P_t^{h,ch} + H_t^{ac} \tag{30}$$

$$H_t^{boiler} = G_t^{boiler} LHV \eta^{boiler} \tag{31}$$

$$P_t^{h,chp} = G_t^{chp} LHV \eta^{h,chp} \tag{32}$$

$$0 \leqslant G_t^{boiler} \leqslant G_{\max}^{boiler} \tag{33}$$

$$0 \leqslant G_t^{chp} \leqslant G_{\max}^{chp} \tag{34}$$

$$0 \leqslant H_t^{ac} \leqslant H_{\max}^{ac} \tag{35}$$

$$0 \leqslant H_t^{boiler} \leqslant H_{\max}^{boiler} \tag{36}$$

$$P_t^{gas} = G_t^{boiler} + G_t^{chp} \tag{37}$$

$$0 \leqslant P_t^{gas} \leqslant p_{\max}^{gas} \tag{38}$$

$$0 \leqslant P_t^{h,chp} + H_t^{boiler} + P_t^{h,disch} - P_t^{h,ch} - H_t^{ac} \leqslant P_{\max}^{h} \tag{39}$$

The generating heat by the boiler and CHP is determined by (31) and (32), respectively. Equations (33) and (34) show the ranges of input gas to the boiler and CHP, respectively. Also, Eq. (36) limits the input heat to the AC. Equation (36) limits the generation of thermal power of the boiler. The imported natural gas and its acceptable ranges are shown in (37) and (38). Finally, the heat pipe limits have been presented in (39).

2.7. Cooling balances

The cooling power balance of SIEMS is presented in (40). The charging power of ISC is described in (41). The output cooling of absorption and electric chillers are shown in (42) and (43), respectively.

$$C_t^{ec} + C_t^{ac} + P_t^{c,disch} = L_t^{c} \tag{40}$$

$$P_t^{c,ch} = P_t^{isc} COP^{isc} \tag{41}$$

$$C_t^{ac} = H_t^{ac} COP^{ac} \tag{42}$$

$$C_t^{ec} = P_t^{ec} COP^{ec} \tag{43}$$

2.8. Water balances and other related constraints

The water balance of SIEMS is shown by (44). Also, the electricity consumption by water section is described in (45) [12].

$$Q_t^{w,w} + Q_t^{d,w} + Q_t^{w,disch} = Q_t^{w,ch} + L_t^{wl} \tag{44}$$

$$P_t^{water,w} = P_t^{d,w} + P_t^{pw,w} + P_t^{ps,w} \tag{45}$$

The SIEMS supplies the freshwater through the underground water and desalination unit. An electric pump is used to mine the underground water. The consumed power of the water well is defined by (46).

$$P_t^{pw,w} = Q_t^{w,w} LL^{w,w} \frac{g^w \rho^w}{\eta^{p,w}(3.6 \times 10^6)} \tag{46}$$

The electricity consumption and produced freshwater of the desalination are described in (47) and (48), respectively.

$$P_t^{d,w} = \eta^{d,w} Q_t^{d,w} \tag{47}$$

$$0 \leqslant Q_t^{d,w} \leqslant Q_{\max}^{d,w} \tag{48}$$

Besides, a water tank is used as the water storage system to create water flexibility for the SIES. The constraints of water tank are shown as follows [12].

$$0 \leqslant Q_t^{w,ch} \leqslant Q_{\max}^{w,ch} WW_t^{w,ch} \tag{49}$$

$$0 \leqslant Q_t^{w,disch} \leqslant Q_{\max}^{w,disch} WW_t^{w,disch} \tag{50}$$

$$L_t^{s,w} = L_{t-1}^{s,w} + \left(\frac{Q_t^{w,ch}}{A^{s,w}}\right) - \left(\frac{Q_t^{w,disch}}{A^{s,w}}\right) \tag{51}$$

$$0 \leqslant L_t^{s,w} \leqslant L_{\max}^{s,w} \tag{52}$$

$$0 \leqslant WW_t^{w,ch} + WW_t^{w,disch} \leqslant 1 \tag{53}$$

Equations (49) and (50) describe the charging and discharging water bounds, respectively. The level of water in storage tank is defined by (51). The acceptable stored water is shown in (52). Also, Eq. (53) determines the charging and discharging modes. Finally, the power consumption of the storage pump is calculated by (54).

$$P_t^{ps,w} = Q_t^{w,ch}\left(L_t^{s,w} + L_{t-1}^{s,w} + LL^{g,w}\right) \frac{g^w \rho^w}{2\eta^{p,w}(3.6 \times 10^6)} \tag{54}$$

3. Multi-layer framework considering generation and demand-side flexibility

The suggested model considers the operating cost, electrical and thermal generation flexibility, and demand-side flexibility simultaneously to present novel scheduling. In the proposed model, the layers evaluates the scheduling of the SIEMS from specific perspectives. The performance of each layer is introduced in the following sub-sections.

3.1. First-layer of the proposed model

This layer focuses on the economic management of the SIEMS. The SIEMS considers the operation cost of power resources, upstream signal prices, and flexibility of loads to minimize total daily operation costs. The cost function of this layer is provided in (55) to (60).

$$\text{Minimize } Cost = Cost^{grid} + Cost^{CHP} + Cost^{boiler} + Cost^{EDR} + Cost^{HDR} \tag{55}$$

$$Cost^{grid} = \sum_t \sum_s \rho_s P_t^g \pi_t^e \tag{56}$$

$$Cost^{boiler} = \sum_t G_t^{boiler} \lambda_t^g \tag{57}$$

$$Cost^{CHP} = \sum_t G_t^{chp} \lambda_t^g \tag{58}$$

$$Cost^{HDR} = \sum_t \left(CR_{dr}^{h,down} PD_t^{h,down} + CR_{dr}^{h,up} PD_t^{h,up}\right) \tag{59}$$

$$Cost^{EDR} = \sum_t \left(CR_{dr}^{e,down} PD_t^{e,down} + CR_{dr}^{e,up} PD_t^{e,up}\right) \tag{60}$$

Equation (55) defines the cost function of the first layer. The imported/selling power costs from/to the main grid has been shown in (56). The operation costs of the boiler and CHP are described in (57) and (58), respectively. Finally, equations (59) and (60) model the costs of the thermal and electrical demand-side management, respectively. The SIEMS performs this scheduling to determine the best operating costs that is donated by *Cost**. The *Cost** is imported to the next step to modify primary scheduling for generation flexibility enhancement.

3.2. Second-layer of the proposed model

The uncertain nature of RES and load demands make new challenges in the operation scheduling of smart energy systems. The flexibility of smart energy systems refers to the ability of the system to manage changes. System flexibility can be achieved in different ways that are categorized into generation and demand-side solutions. This layer focuses on the generation side solutions to simultaneously increase the electrical and thermal generation. More reservation enhances generation flexibility. Therefore, this layer efforts to maximize the electrical and thermal spinning reserves while supplying the required demands. At this layer, the first layer scheduling has been modified according to (61):

$$\begin{aligned} &\text{Maximum} \sum_t \left[ES_t^e + \left(P_{\max}^{e,chp} - P_t^{e,chp}\right)\right] + \sum_t \left[ES_t^h + \left(P_{\max}^{h,chp} - P_t^{h,chp}\right)\right] \\ &\qquad Subject\ to: \\ &\qquad Cost \leqslant \gamma Cost^* \\ &\qquad Equations\ (1) - (60) \end{aligned} \tag{61}$$

The first term $ES_t^e + \left(P_{max}^{e,chp} - P_t^{e,chp}\right)$ refers to the electrical generation flexibility (EGF) and the second term $ES_t^h + \left(P_{max}^{h,chp} - P_t^{h,chp}\right)$ shows the thermal generation flexibility (TGF). As we can see, the CHP and storage systems are considered to create generation flexibility, while the upstream network, boiler, and RES supply the required demand loads. It is worth to mention a little margin $\gamma \geq 1$ is introduced for the second layer to keep the optimal operating costs in the acceptable ranges while increasing the generation flexibility. The optimal generation flexibility is determined by the second layer which is shown as *GF**.

3.3. Third-layer of the proposed model

Similar to the second layer, this layer focuses on the SIEMS flexibility with the difference that the third layer studies the flexibility of end-users. The DR programs are the solution to provide flexibility for end-users. When the generating power of RES changes from the forecasted values, the customers can reduce their consumption by load shifting. Therefore, the SIEMS establishes the power balance, and the system remains stable. The main challenge of DR programs is that their uncoordinated implementation may cause new peak loads. The new peak load is usually created when the electricity prices are low. At these times, the local resources must generate more power to supply the required demands. Therefore, the spinning reserve significantly decreases, and it has a negative impact on the generation flexibility. For this reason, this layer effort to reschedule the operation planning of the SIEMS aiming to uniform load profile. The third stage optimization problem is defined according to (62):

$$\begin{aligned} &\text{Min - Max } P_t^{e,load} + \text{Max - Min } P_t^{e,load} \\ &Subject\ to: \\ &GF \geqslant \theta GF^* \\ &\text{Cost} \leqslant \gamma \text{Cost}^* \\ &Equations\ (1)-(61) \\ &P_t^{e,load} = L_t^e + PD_t^{e,up} - PD_t^{e,down} \end{aligned} \tag{62}$$

The optimization problem is modeled as the hybrid min–max and max-max approaches. The term min–max decreases the peak, while the term max–min increases the minimum load. Considering both terms uniforms the load profile. Also, the constant parameter $\theta \leq 1$ is defined to determine the search area in the third layer. Therefore, the final operation scheduling of SIEMS is determined by this layer. Fig. 2 shows the relationship between the three layers.

4. Flexibility indexes

In this paper, we introduce three novel indexes to evaluate the performance of different energy scheduling frameworks on the flexibility of SIMES. To this end, the average electrical generation flexibility index (*AEGFI*) and the average thermal generation flexibility index (*ATGFI*) are defined by (63) and (64) to show the electrical and thermal generation flexibility of SIEMS during day-ahead scheduling.

$$AEGFI = \frac{1}{N_t}\sum_{t=1}^{N_t} SoC_t^e + (P_{max}^{CHP} - P_t^{CHP}) \tag{63}$$

$$ATGFI = \frac{1}{N_t}\sum_{t=1}^{N_t} SoC_t^h + (H_{max}^{CHP} - H_t^{CHP}) \tag{64}$$

The large value of two indexes enhances the ability of the SIEMS to control the uncertainty of renewable resources. Also, we proposed the average demand-side flexibility during the peak period index (*ADFPPI*) to show the demand-side flexibility of SIEMS by (65).

$$ADFPPI = \frac{1}{N_{t\in p}}\sum_{t=1}^{N_{t\in p}} (P_t^{base} - P_t^{EDR}) \tag{65}$$

Where $t \in p$ denotes to the peak periods. This index shows how the SIEMS participates in demand-side flexibility by load reduction during peak periods.

5. Case studies and simulation results

5.1. Input data

The proposed multi-layer day-ahead operation framework is tested on a standard SIES. The maximum energy exchange with grid is assumed 700 kW. The maximum purchased gas from the gas network is 3400 m^3. The characteristics of ice storage, thermal storage, and electrical storage systems are presented in Table 1. The maximum level of the water storage system is 19.6 m [12]. The water pump efficiency and the maximum capacity of the desalination unit are 85% and 25 m3/h, respectively.

The electrical and thermal efficiencies of the CHP unit are 35% and 45%, respectively. The efficiency and maximum generating heat power of the boiler are 80% and 20 kW, respectively. Seven scenarios were generated to consider the probabilistic nature of renewable generation, loads, and prices. Different scenarios are presented in Figs. 3–6. The electricity prices are taken from the PJM market [37]. Also, the gas price is assumed that 22 cents/m^3 which is taken from [38].

5.2. Case studies

Two following case studies are performed on the SIEMS to show the efficiency, reliability, and superiority of the proposed multi-layer framework:

Table 1
Energy storage systems characteristics.

Energy storage	$E^i_{min}(kWh)$	$E^i_{max}(kWh)$	$P^{i,ch}_{max}(kW)$	$P^{i,disch}_{max}(kW)$	$\eta^{i,ch}\eta^{i,disch}(\%)$
Thermal	10	100	20	20	98
Electrical	10	100	20	20	96
Ice storage	800	1800	700	800	95–97

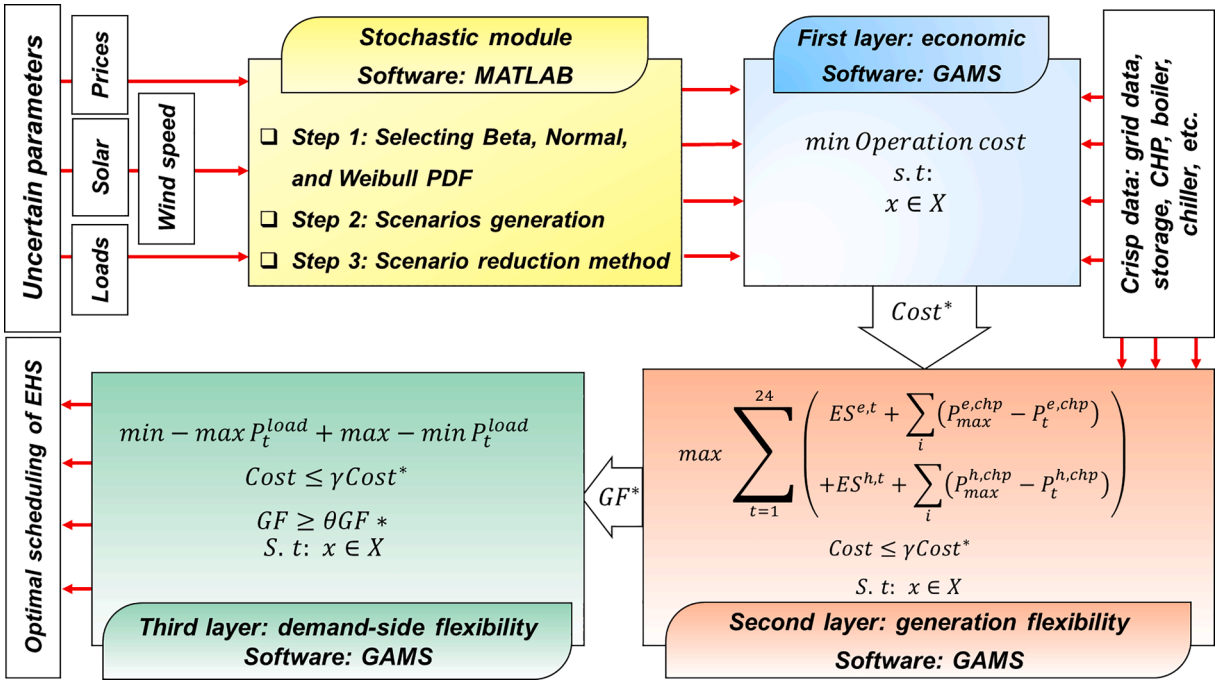

Fig. 2. Multi-layer operation planning framework.

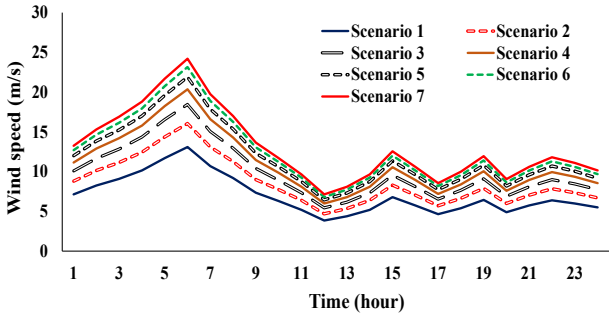

Fig. 3. Different scenarios for wind speed.

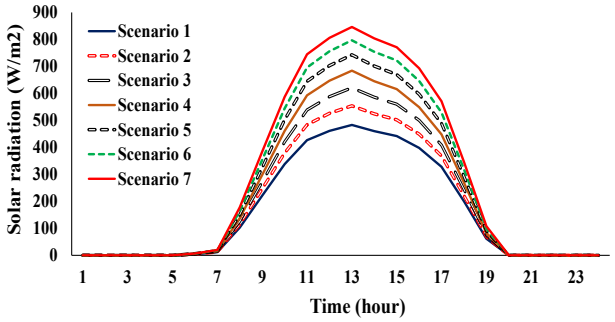

Fig. 4. Different scenarios for solar radiation.

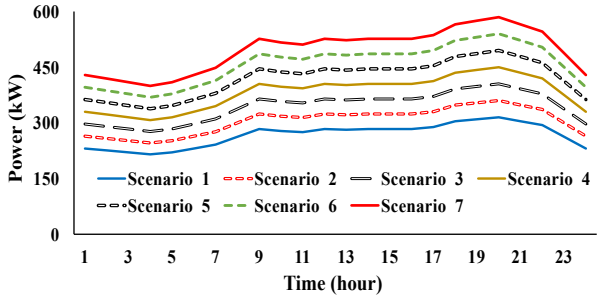

Fig. 5. Different scenarios for load.

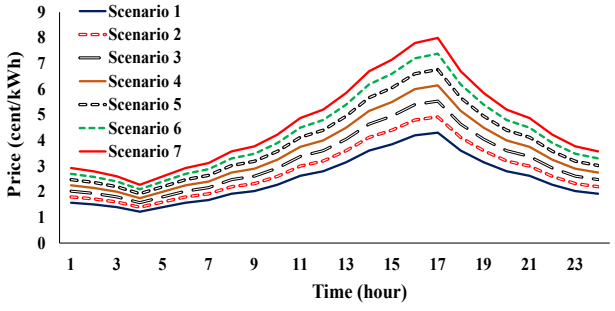

Fig. 6. Different scenarios for market price.

- ***Case study 1:*** In this case study, general operation planning is performed so that SIEMS minimizes the total day-ahead costs considering the integration of renewable energy, different energy storage systems, and electrical and thermal DR programs. It is worth mentioning that the generation and demand-side flexibilities are not considered objective functions.
- ***Case study 2:*** In this case study, SIEMS performs the suggested framework Fig. 2 to improve the operating costs, thermal generation flexibility (*TGF*), electrical generation flexibility (*EGF*), and demand-side flexibility simultaneously. Table 2 shows the simulation results for case studies.

The simulation results show that the *AEGFI* reaches from 127.43 kWh to 156.73 kWh in the multi-layer model. Also, the multi-layer framework increases the *ATGFI* from 124.25 kWh to 167.29 kWh. Since the second layer of focuses to increase the generation flexibility, the *AEGFI* and *ATGFI* are improved by 22.98% and 34.64% compared to case study 1, respectively.

Also, the results show that the multi-layer framework significantly increases *ADFPPI*. The *ADFPPI* in case 1 is 19.39 kWh, while the proposed model increases by 65.75%, and *ADFPPI* reaches 32.14 kWh. Table 3 compares the load profile characteristics.

As can be seen, the proposed multi-layer model significantly reduces the peak load. Given that the third layer attempts to uniform the load profile, the load factor and peak load have been improved. The peak load in case 1 is 461.95 kW which has been reduced by the proposed model by 12.34%. However, the suggested model increases the load factor by 14.07% through the proposed hybrid - min–max and max–min approaches. Besides, Table 3 shows when the uncoordinated DR program was performed, it may generate a new peak during the off-peak period. When DR programs were not implemented, the peak load is 449.95 kW while it increased with the uncoordinated DR program in case 1 to 461.95 kW. It is worth mentioning that smoothing the load profile increases the system flexibility because the peak load is reduced. Therefore, the spinning reservation increases during peak hours, and SIEMS has more capability to control the uncertainty of RES. Fig. 7 presents the electrical load profile for two case studies.

Fig. 7 shows that the load profile in case 2 is more uniform than in case 1. As we can see, case 1 creates a new peak because the electricity prices are low during off-peak periods. Actually, SIEMS transfers most of its consumption to the off-peak period to reduce operating costs. While in the multi-layer model, the load profile has better performance. Figs. 8 and 9 compare the electrical and thermal generation flexibility of case studies.

The simulation results show that the electrical and thermal flexibility in case 2 is more than in case 1. According to Fig. 8, SIEMS has no flexibility during hours 18 to 21 in case study 1, while in the proposed model, there is at least 100 kWh of flexibility at each time slot. Besides, in terms of thermal generation flexibility, the suggested approach has better performance. In case 1 the thermal flexibility at hours 10 and 11 is zero, while the thermal flexibility of the SIEMS in the proposed model is more than 100 kWh at each time slot. Therefore, in the suggested approach, the SIEMS has more capability to manage the uncertainty of RES and load demand. Also, the flexibility enhancement allows the SIEMS to be more resilient in emergency situations.

5.3. Energy balances

In this section, the electrical, thermal, cooling, and water balances for the proposed multi-layer framework are studied. Fig. 10 presents the electrical power balance.

It can be observed that most of the required electricity energy has been provided by the main grid and CHP unit because of high efficiencies. Also, it can be easily observed that SIEMS participates in electrical DR programs and shifts their loads to off-peak hours. These programs help the peak load reduction and provide a cost-saving opportunity for the SIES. Also, the ice storage conditioner is fully charged when the prices are low. It converts the electrical energy to cooling energy and discharges the stored cooling energy during peak hours. However, EESS is fully charged at t1 to t5 to provide maximum flexibility for the SIES. Fig. 11 presents the hourly thermal power balance.

Table 2
Simulation results of two case studies.

Case studies	*Cost ($)*	*AEGFI(kWh)*	*ATGFI(kWh)*	*ADPPFI(kWh)*	*Emission (kg)*
Case study 1	82499.06	127.43	124.25	19.39	16036.2
Case study 2	86233.37	156.71	167.29	32.14	15997.1
Improvement (%)	−4.52	+22.98	+34.64	+65.75	+0.244

Table 3
Load profile characteristics.

Case studies	Peak (kW)	Valley (kW)	PAR (p. u)	L.F. (%)	*ADPPFI*(kWh)
Base load	449.95	307.47	1.18	8479	0
Case study 1	461.95	338.22	1.21	82.59	19.39
Case study 2	404.96	338.22	1.06	94.21	32.14
Improvement (%)	+12.34	0	+12.4	+14.07	+65.75

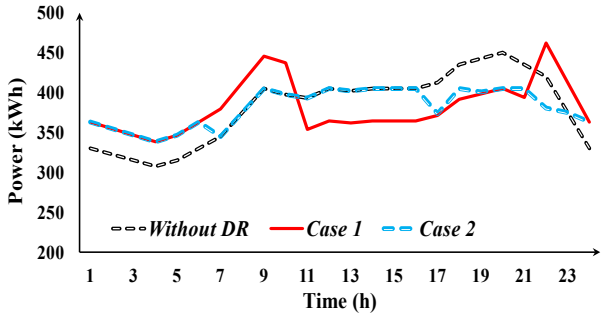

Fig. 7. Load profile of SIES.

Fig. 11 shows that the CHP unit has the largest share of thermal energy generation due to its high efficiency. Due to its low capacity and low efficiency, the boiler unit is used to supply a part of thermal energy at some hours. Also, according to the figure, the TESS is charged during off-peak hours to SIEMS discharges the stored energy during peak hours. The cooling and water balances are presented in Figs. 12 and 13, respectively.

Fig. 12 shows that the electric chiller and ice storage conditioner supply the required cooling energy for SIES. The ice storage conditioner is charged during off-peak hours by electrical power. It converts the electrical energy to cooling energy to supply the required energy during peak hours. Since the COP of the absorption chiller is less than the electric chiller, SIEMS prefers to provide the more energy by the electric chiller. According to Fig. 13, the SIEMS extracts the maximum fresh water from the underground water resources by water pump because it consumes less electricity rather than the desalination. Since the desalination unit consumes more electrical energy, SIEMS utilizes it during peak times to provide the required fresh water.

5.4. Sensitivity analysis

In this section, we present a sensitivity analysis to show the performance of the proposed multi-layer model in different conditions. Table 4 shows the impact of gas price on the performance of the suggested approach and single-objective optimization problem. The gas price is changed from 22 cents/m^3 to 30 cents/m^3, and the simulation results are presented in Table 4.

Results demonstrated that the suggested approach provides more electrical and thermal generation flexibility compared to single-objective framework. According to Table 4, the AEGFI and ATGFI are improved by at least 24.28% and 38.10% in the proposed model, respectively. These improvements have been achieved because the second layer of the suggested model emphasizes to maximize both electrical and thermal flexibilities. Table 5 demonstrates the impacts of electricity prices on the performance of two case studies. The "electricity price coefficient" has been defined that show the scale of electricity prices compared to base electricity prices (the base electricity prices are shown in Fig. 6).

The simulation results show that as the coefficient increases (electricity price increases), the AEGFI and ATGFI decrease in the single-objective model. These indexes have been decreased because the SIEMS prefers to provide the needed energy with local resources to reduce operating costs. But, in the suggested approach, the AEGFI and ATGFI are independent of the electricity prices and fixed at 163.47 kWh and 174.03 kWh, respectively. The simulation results show that based on different conditions, the suggested approach can improve the AEGFI and ATGFI by 49.27% and 114.01%, respectively.

The charging and discharging efficiency of EES is increased from 80% to 100% and the simulation results have been presented in Table 6. As efficiency increases, the cost of SIMES is reduced because ESS will have less power loss. When the efficiency of ESS is 80%, the operating cost of SIMES is $ 82618.25, while it has decreased to $ 82471.52 in

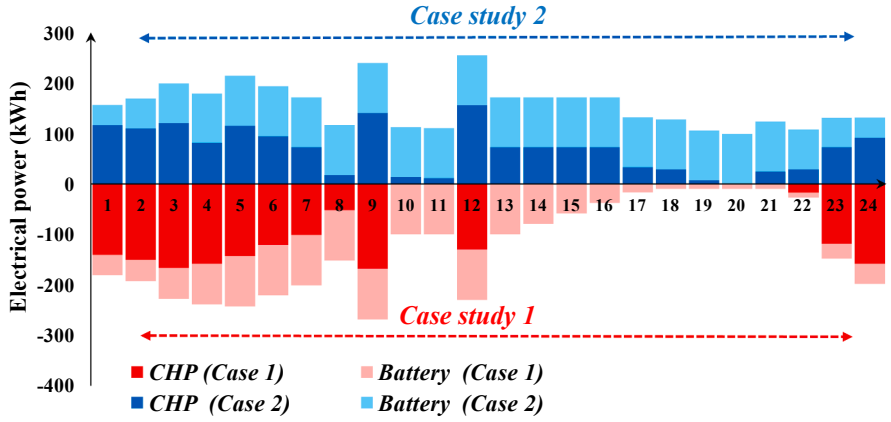

Fig. 8. Electrical generation flexibility.

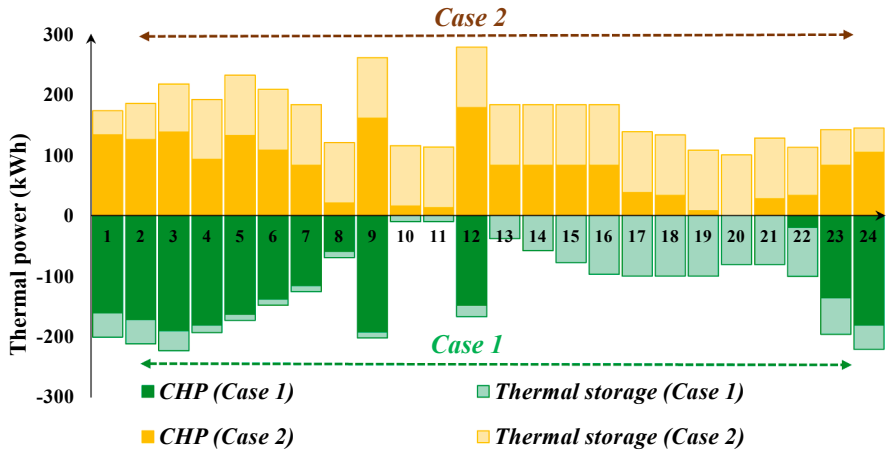

Fig. 9. Thermal generation flexibility.

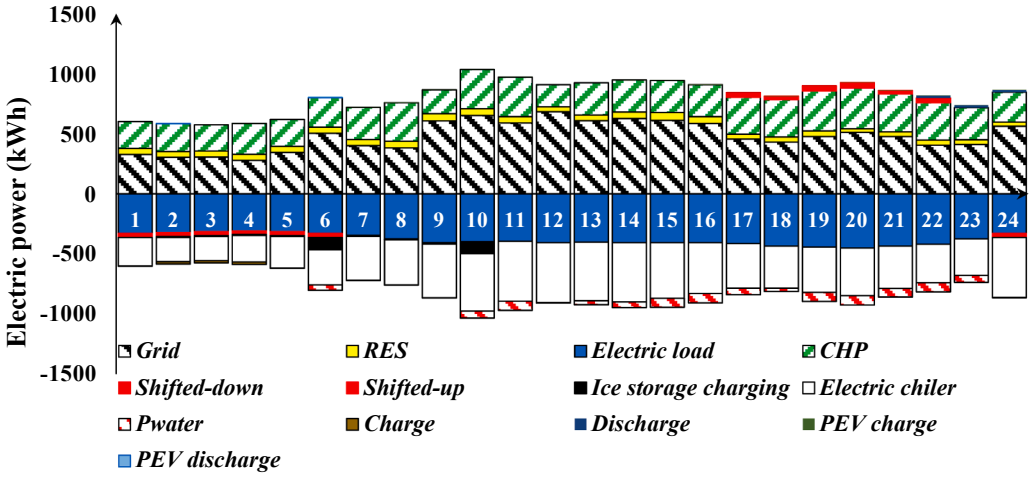

Fig. 10. Electrical power balance of SIEMS in case2.

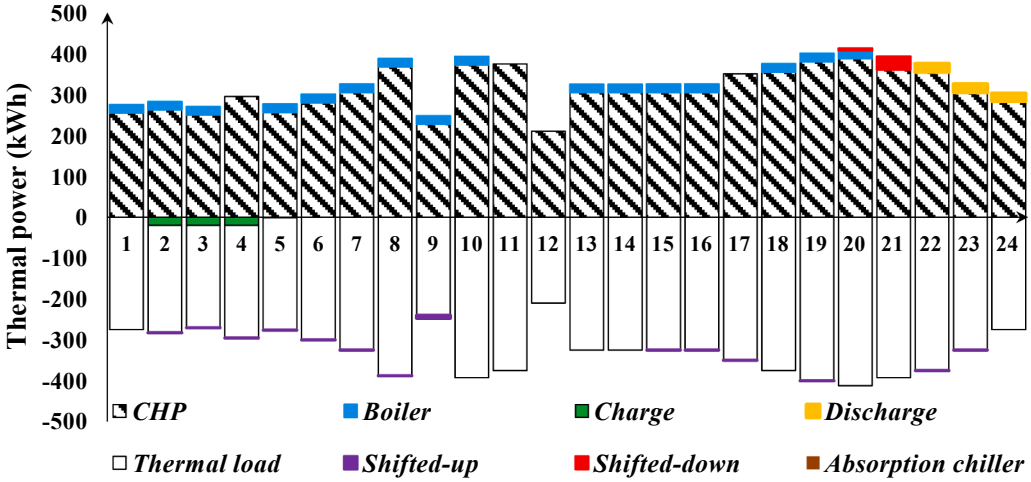

Fig. 11. Thermal power balance of SIEMS in case2.

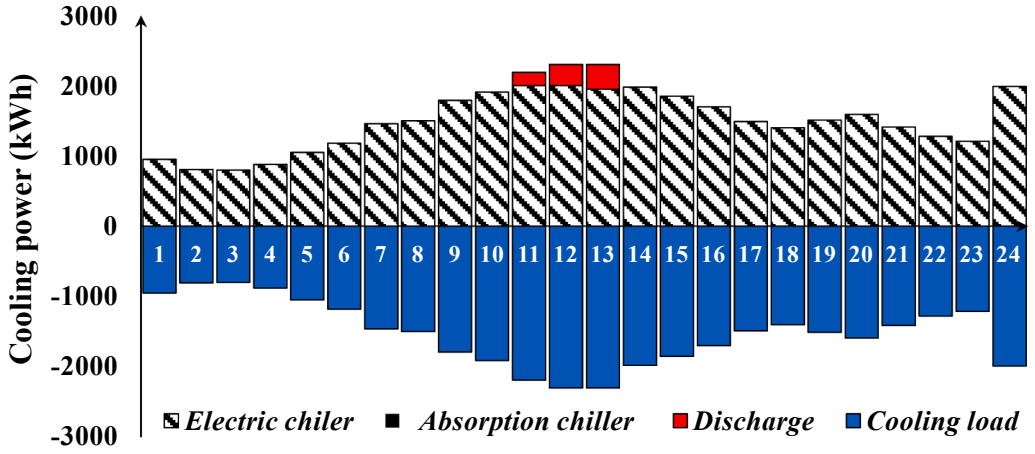

Fig. 12. Cooling balance of SIEMS in case2.

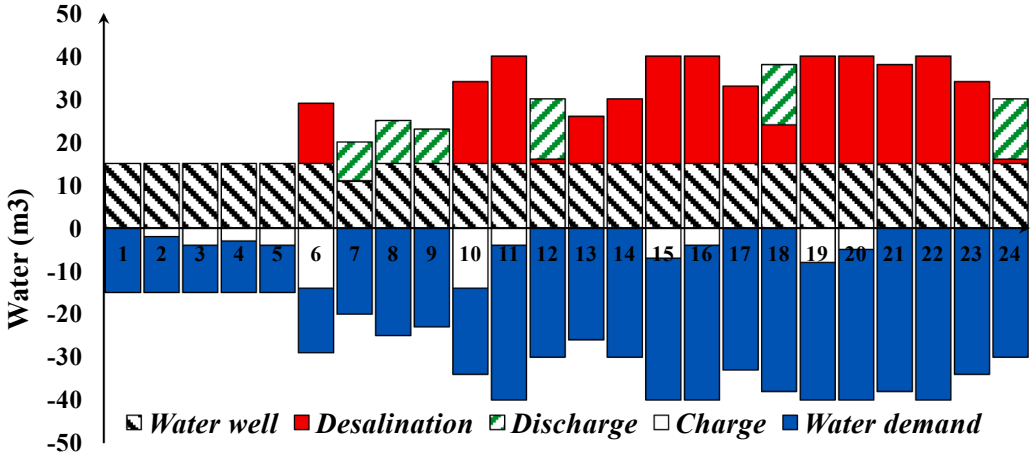

Fig. 13. Water balance of SIEMS in case2.

Table 4
Sensitivity analysis on gas prices.

Gas price (cents/m^3)	*AEGFI*(kWh)			*ATGFI*(kWh)		
	Single objective	Proposed multi-layer	Improvement	Single objective	Proposed multi-layer	Improvement
22	127.43	163.47	28.28 %	124.25	174.03	40.06 %
24	130.56	163.47	25.21 %	124.76	174.03	39.49 %
26	131.53	163.47	24.28 %	124.47	174.03	39.82 %
28	130.02	163.47	25.73 %	124.65	174.03	39.61 %
30	131.04	163.47	24.75 %	126.02	174.03	38.10 %

Table 5
Sensitivity analysis on electricity prices.

Electricity price coefficient	*AEGFI(kWh)*			*ATGFI(kWh)*		
	Single objective	Proposed multi-layer	Improvement	Single objective	Proposed multi-layer	Improvement
1	127.43	163.47	28.28%	124.25	174.03	40.06%
1.1	122.49	163.47	33.46%	117.50	174.03	48.11%
1.2	114.73	163.47	42.48%	110.33	174.03	57.74%
1.3	109.51	163.47	49.27%	95.62	174.03	82.00%
1.4	109.52	163.47	49.26%	81.32	174.03	114.01%

Table 6
Sensitivity analysis on charging/discharging efficiency of ESS.

Charging and discharging efficiency	Cost ($)	*AEGFI(kWh)*			*ATGFI(kWh)*		
		Single objective	Proposed multi-layer	Improvement	Single objective	Proposed multi-layer	Improvement
80%	82618.25	128.11	163.19	27.38%	124.67	174.03	39.59%
85%	82579.19	127.45	163.26	28.10%	124.67	174.03	39.59%
90%	82541.88	127.12	163.34	28.49%	123.64	174.03	40.76%
95%	82506.07	127.38	163.45	28.32%	123.40	174.03	41.03%
100%	82471.52	129.28	163.57	26.52%	124.46	174.03	39.83%

efficiency 100%. However, the results demonstrated that the flexibility indexes in the suggested approach are higher than in case study 1 (single-objective optimization). According to Table 6, the suggested approach improves the AEGFI and ATGFI indexes by at least 26.52% and 39.59%, respectively.

6. Conclusion

This paper suggested a multi-layer operation framework to present the optimal management for smart integrated energy systems. The proposed structure integrated the electrical, thermal, cooling, and water sectors to increase the efficiency of the smart energy system. The multi-layer framework simultaneously optimizes the operating costs, thermal generation flexibility, electrical generation flexibility, and demand-side flexibility. At the first layer, the smart integrated energy system considers the uncertainty of load demand, RES, and signal prices to minimize total operating costs. The second layer tries to increase the thermal and electrical generation flexibilities to facilitate the integration of renewable energy resources as much as possible. The third layer applied the hybrid min–max and max–min approaches to increase the demand-side flexibility through load profile smoothing. With the uniformity of the load profile, the integrated energy system will have a suitable reserve capacity at each time slot, which increases the system's flexibility. The results illustrate that the stochastic tri-layer framework increases *AEGFI*, *ATGFI*, and *ADPPFI* by 22.98%, 34.64%, and 65.75%, respectively. Also, it prevents the new peak in the load profile and improves the load factor and peak-to-average ratio to 94.21% and 1.06p.u, respectively. We will evaluate the tri-layer framework on networked smart energy systems in the future work.

7. Intellectual property

We confirm that we have given due consideration to the protection of intellectual property associated with this work and that there are no impediments to publication, including the timing of publication, with respect to intellectual property.

Funding

This work is based upon research funded by Iran National Science Foundation (INSF) under project No.4013185.

CRediT authorship contribution statement

Hamid Karimi: Conceptualization, Data curation, Formal analysis, Methodology, Software, Validation, Project administration, Supervision, Writing – original draft. **Shahram Jadid:** Methodology, Project administration, Supervision, Writing – review & editing.

Declaration of Competing Interest

The authors declare that they have no known competing financial interests or personal relationships that could have appeared to influence the work reported in this paper.

Data availability

Data will be made available on request.

Acknowledgement

This work is based upon research funded by Iran National Science Foundation (INSF) under project No.4013185.

References

[1] Akbarian A, Andooz A, Kowsari E, Ramakrishna S, Asgari S, Cheshmeh ZA. Challenges and opportunities of lignocellulosic biomass gasification in the path of circular bioeconomy. Bioresour Technol 2022;362:127774.
[2] de Mendonça, Henrique Vieira, Paula Assemany, Mariana Abreu, Eduardo Couto, Alyne Martins Maciel, Renata Lopes Duarte, Marcela Granato Barbosa dos Santos, and Alberto Reis. "Microalgae in a global world: new solutions for old problems?" Renewable Energy, vol. 165, 842-862.
[3] Li J, Yang L. Back side of the coin: How does non-fossil energy diffusion result in less efficient fossil-based technologies. Environ Impact Assess Rev 2022;96:106848.
[4] Huang Z, Guo Z, Ma P, Wang M, Long Y, Zhang M. Economic-environmental scheduling of microgrid considering V2G-enabled electric vehicles integration. Sustainable Energy Grids Networks 2022;32:100872.
[5] Mahone A, Subin Z, Orans R, Miller M, Regan L, Calviou M, et al. On the path to decarbonization: Electrification and renewables in California and the Northeast United States. IEEE Power Energ Mag 2018;16(4):58–68.
[6] Algunaibet IM, Pozo C, Galán-Martín Á, Guillén-Gosálbez G. Quantifying the cost of leaving the Paris Agreement via the integration of life cycle assessment, energy systems modeling and monetization. Appl Energy 2019;242:588–601.
[7] Paliwal P. Multi-Stage Framework for Analyzing Penetration of Stochastic Distributed Energy Resources and Storage. Iranian Journal of Electrical and Electronic Engineering 2022;18(4):2258.
[8] Chang, Lei, Hayot Berk Saydaliev, Muhammad Saeed Meo, and Muhammad Mohsin. "How renewable energy matter for environmental sustainability: Evidence from top-10 wind energy consumer countries of European Union." Sustainable Energy, Grids and Networks, vol. 31, 2022, 100716.
[9] Heidari A, Mortazavi SS, Bansal RC. Stochastic effects of ice storage on improvement of an energy hub optimal operation including demand response and renewable energies. Appl Energy 2020;261:114393.
[10] Huang W, Zhang Xi, Li K, Zhang N, Strbac G, Kang C. Resilience Oriented Planning of Urban Multi-Energy Systems With Generalized Energy Storage Sources. IEEE Transactions on Power System 2022;37(4):pp.
[11] Wang Ni, Liu Z, Heijnen P, Warnier M. A peer-to-peer market mechanism incorporating multi-energy coupling and cooperative behaviors. Appl Energy 2022;311:118572.
[12] Pakdel MJ, Vahid FS, Mohammadi-Ivatloo B. Multi-objective optimization of energy and water management in networked hubs considering transactive energy. J Clean Prod 2020;266:121936.
[13] Hu K, Wang B, Cao S, Li W, Wang L. A novel model predictive control strategy for multi-time scale optimal scheduling of integrated energy system. Energy Rep 2022;8:7420–33.
[14] Wang L, Shi Z, Dai W, Zhu L, Wang X, Cong H, et al. Two-stage stochastic planning for integrated energy systems accounting for carbon trading price uncertainty. Int J Electr Power Energy Syst 2022;143:108452.
[15] Wang Y, Yuli Zhang Lu, Xue CL, Song F, Sun Y, Liu Y, et al. Research on planning optimization of integrated energy system based on the differential features of hybrid energy storage system. J Storage Mater 2022;55:105368.
[16] Karimi H, Jadid S, Hasanzadeh S. A stochastic tri-stage energy management for multi-energy systems considering electrical, thermal, and ice energy storage systems. J Storage Mater 2022;55:105393.
[17] Lasemi MA, Arabkoohsar A, Hajizadeh A, Mohammadi-Ivatloo B. A comprehensive review on optimization challenges of smart energy hubs under uncertainty factors. Renew Sustain Energy Rev 2022;160:112320.
[18] Kaushik E, Prakash V, Mahela OP, Khan B, El-Shahat A, Abdelaziz AY. Comprehensive overview of power system flexibility during the scenario of high penetration of renewable energy in utility grid. Energies 2022;15(2):516.

[19] Honarmand HA, Rashid SM. A sustainable framework for long-term planning of the smart energy hub in the presence of renewable energy sources, energy storage systems and demand response program. J Storage Mater 2022;52:105009.
[20] Tiwari S, Singh JG. Optimal energy management of multi-carrier networked energy hubs considering efficient integration of demand response and electrical vehicles: A cooperative energy management framework. J Storage Mater 2022;51:104479.
[21] Rahgozar S, Seyyedi AZG, Siano P. A resilience-oriented planning of energy hub by considering demand response program and energy storage systems. J Storage Mater 2022;52:104841.
[22] Rezaei S, Ghasemi A. Stochastic scheduling of resilient interconnected energy hubs considering peer-to-peer energy trading and energy storages. J Storage Mater 2022;50:104665.
[23] Palani V, Vedavalli SP, Veeramani VP, Sridharan S. Optimal operation of residential energy Hubs include Hybrid electric vehicle & Heat storage system by considering uncertainties of electricity price and renewable energy. Energy 2022; 261:124952.
[24] Karimi H, Jadid S, Hasanzadeh S. Optimal-sustainable multi-energy management of microgrid systems considering integration of renewable energy resources: A multi-layer four-objective optimization. Sustainable Production and Consumption 2023;36:126–38.
[25] Wen P, Xie Y, Huo L, Tohidi A. Optimal and stochastic performance of an energy hub-based microgrid consisting of a solar-powered compressed-air energy storage system and cooling storage system by modified grasshopper optimization algorithm. Int J Hydrogen Energy 2022;47(27):13351–70.
[26] Tavakoli A, Karimi A, Shafie-khah M. Optimal probabilistic operation of energy hub with various energy converters and electrical storage based on electricity, heat, natural gas, and biomass by proposing innovative uncertainty modeling methods. J Storage Mater 2022;51:104344.
[27] Thang VV, Ha T, Li Q, Zhang Y. Stochastic optimization in multi-energy hub system operation considering solar energy resource and demand response. Int J Electr Power Energy Syst 2022;141:108132.
[28] Mansouri SA, Ahmarinejad A, Sheidaei F, Javadi MS, Rezaee Jordehi A, Esmaeel Nezhad A, et al. A multi-stage joint planning and operation model for energy hubs considering integrated demand response programs. Int J Electr Power Energy Syst 2022;140:108103.
[29] Mansouri, Seyed Amir, Emad Nematbakhsh, Amir Ahmarinejad, Ahmad Rezaee Jordehi, Mohammad Sadegh Javadi, and Seyed Alireza Alavi Matin. "A multi-objective dynamic framework for design of energy hub by considering energy storage system, power-to-gas technology and integrated demand response program." Journal of Energy Storage 2022; 50: 104206.
[30] Nasir M, Jordehi AR, Tostado-Veliz M, Tabar VS, Mansouri SA, Jurado F. Operation of energy hubs with storage systems, solar, wind and biomass units connected to demand response aggregators. Sustain Cities Soc 2022;83:103974.
[31] Bahmani R, Karimi H, Jadid S. Cooperative energy management of multi-energy hub systems considering demand response programs and ice storage. Int J Electr Power Energy Syst 2021;130:106904.
[32] Dorahaki S, Abdollahi A, Rashidinejad M, Moghbeli M. The role of energy storage and demand response as energy democracy policies in the energy productivity of hybrid hub system considering social inconvenience cost. J Storage Mater 2021;33: 102022.
[33] Miao P, Yue Z, Niu T, Alizadeh As'ad, Jermsittiparsert Kittisak. Optimal emission management of photovoltaic and wind generation based energy hub system using compromise programming. J Clean Prod 2021;281:124333.
[34] Jadidbonab M, Babaei E, Mohammadi-ivatloo B. CVaR-constrained scheduling strategy for smart multi carrier energy hub considering demand response and compressed air energy storage. Energy 2019;174:1238–50.
[35] Nojavan S, Saberi K, Zare K. Risk-based performance of combined cooling, heating and power (CCHP) integrated with renewable energies using information gap decision theory. Appl Therm Eng 2019;159:113875.
[36] Allahvirdizadeh Y, Galvani S, Shayanfar H. Data clustering based probabilistic optimal scheduling of an energy hub considering risk-averse. Int J Electr Power Energy Syst 2021;128:106774.
[37] Nguyen DT, Nguyen HT, Le LB. Dynamic pricing design for demand response integration in power distribution networks. IEEE Trans Power Syst 2016;31(5): 3457–72.
[38] Lu X, Liu Z, Ma Li, Wang L, Zhou K, Feng N. A robust optimization approach for optimal load dispatch of community energy hub. Appl Energy 2020;259:114195.